ARTICLES

Fullerenes in Photoconductive Polymers. Charge Generation and Charge Transport

Ying Wang* and Andris Suna

Central Research and Development, Du Pont Co., P.O. Box 80356, Wilmington, Delaware 19880-0356

Received: December 9, 1996[⊗]

Fullerenes enhance the photoconductivity of photoconductive polymers. This paper studies the mechansim of enhancement both experimentally and theoretically. The effects of fullerene doping on the spectroscopic, charge generation, and charge transport properties of the polymer are reported. Electrical field effects and magnetic field effects are examined. On the basis of these data a charge generation mechansim involving a singlet of weak charge-transfer complex is proposed for fullerene-doped *N*-poly(vinylcarbazole). A new theoretical model combining both the Onsager and Marcus theory is developed to quantitatively account for the field-dependent charge generation efficiency in nonpolar medium.

Fullerenes, C_{60} and C_{70},[1] are known to be good electron acceptors.[2,3] They can form charge-transfer complexes[4,5] or charge-transfer salts[6] with electron donors such as aromatic amines. Ferromagnetism[6] and enhanced second-order optical nonlinearity[7] have been observed from these charge transfer complexes. The direct optical excitation of fullerene can lead to excited state electron transfer reactons,[4,5,8−16] which is the basis of photoconductivity.

The first fullerene-based polymeric photoconductor was demonstrated by doping fullerenes into polymers containing electron-donating moieties such as *N*-poly(vinylcarbazole) (PVK).[17,18] The enhancement effects of fullerenes on the photoconductivity of polymers were also reported for phenylmethylpolysilane (PMPS),[19] poly(*p*-phenylenevinylene),[20] poly(3-alkylthiophene),[21] and poly(2,5-dialkoxy-*p*-phenylenevinylene).[22] The enhanced photoconductivity is attributed to the electron transfer reaction between fullerene and polymer. The quantum yields of charge generation at high fields for fullerene-doped PVK and PMPS are close to unity.[17,19a] Recently, by doping fullerenes into optically nonlinear polymers, photorefractive effects have been observed.[23,24] Because of all these novel optoelectronic phenomena displayed by fullerene, a detailed understanding of the photoconducting mechanism of fullerene in polymers is of great importance.

The purpose of this paper is to study the effects of fullerene doping on the charge transport and charge generation properties of the host photoconductive polymer. It will be shown that the effects of fullerene doping on the hole transport property of the polymer are minimal. So the main focus of the paper will be on the charge generation mechanism of fullerene-doped polymeric photoconductors, in particular, fullerene-doped PVK.

It is known that, upon photoexcitation, the singlet state of C_{60} and C_{70} undergoes efficient intersystem crossing to generate a long-lived triplet state (lifetime varies from micro- to milliseconds depending on the conditions) with a quantum yield of almost 1.[25−27] In solutions, where the diffusion of reactants to close distance is required for reactions to occur, the long-lived triplet state is therefore expected to be the main precursor for charged carrier generation. In polymer, however, the situation is very different. The reactants are already close to each other, so even the short-lived singlet state can have time to react with the neighboring molecules before decaying to the triplet state. This is the case with fullerene-doped PVK where the carbazole moiety, an electron donor, exists in high concentration with an average separation distance of ∼6.4 Å.[28] Both singlet and triplet state can in principle participate in the electron transfer reactions in PVK film. In addition, the precursor for the generation of charge carriers may be the excited states of either PVK, fullerene, or the complexes of the two. These are the issues that will be addressed here.

This paper also address a more general issue regarding the quantitative treatment of charge generation processes in polymers. The field-dependent charge separation theory of Onsager[29] has been the standard model to use for analyzing the charge generation efficiency of polymeric photoconductors for many years, in spite of its generally recognized deficiencies. The theory predicts the probability of an electron−hole (e−h) pair separating to infinity by solving the diffusion equation of the relative motion of the e−h pair in the potential provided by their Coulomb interaction and applied external field. The origin of the e−h pair and the pathway by which it is generated are not considered in the model. An important boundary condition (and an assumption) for this model is that if the e−h pair separation distance reaches zero, the pair annihilates (with an infinitively fast rate). For low dielectric constant solids, the theory predicts a strong field-dependent charge generation efficiency depending on the initial e−h separation distance. The shorter the initial separation distance, the stronger the field dependence.

Over the past decades, the field-dependent charge generation efficiency of many polymeric photoconductors have been fitted to the Onsager theory with apparent success.[30−34] However, fairly large initial e−h separation distances (20−40 Å) have to be assumed for the Onsager theory to fit these data, as in the cases of fullerene-doped polymers studied here.[17−19] As already recognized by previous workers[35−38] and discussed in details elsewhere,[35,36] this is a puzzling result. In inorganic systems, large initial e−h separation distance is usually rationalized as the distance required for the excess energy of electron and hole to thermalize. However, this is less likely in molecular systems because the internal conversion process from higher excited

[⊗] Abstract published in *Advance ACS Abstracts,* July 1, 1997.

S1089-5647(96)04019-9 CCC: $14.00

states to the lowest excited state is very efficient due to the availability of high-frequency phonons and strong electron−phonon coupling. In fact, in many cases it was concluded experimentally that the charge-transfer state is responsible for the charge generation, which should lead to an initial e−h separation distance of only a few angstroms.[35,36]

This paradox indicates the inadequacy of the assumption used in the Onsager model that the e−h pair annihilates instantaneously when their separation distance reaches zero. This assumption is unrealistic in the real system. For an e−h pair to recombine to the ground state, energy on the scale of electronvolts has to be disposed of, usually dumped into the vibrational modes of the system. This is a process with finite rate. Because of the assumption of an unrealistically large recombination rate, an unrealistically large value of the initial e−h separation distance has to be used for the Onsager model to fit the data. Furthermore, the creation and recombination rate may depend on the field, separation distance, and energetics. None of these is considered by the Onsager model.

The need for a finite recombination rate was recognized by Braun[35] and Noolandi and Hong.[36] Braun proposed a kinetic model which identifies the geminate e−h pair with the excited charge-transfer state, which typically has lifetime on the scale of nanoseconds.[35] The lifetime of the charge transfer state, which corresponds to the charge recombination step, is assumed to be field-independent. The dissociation rate is assumed to be field-dependent and follows the formula for either classical ion pair or Wannier exciton. Braun's model is a special case of a more general model of Noolandi and Hong.[36] They give the exact solution of the electron and hole escape probability corresponding to a partly absorbing sphere of finite radius at the origin. Indeed, by assuming a slow recombination rate (taken to be the lifetime of either the charge transfer state or the singlet state), the field-dependent charge generation data can be fitted by these modified Onsager models with small initial e−h separation distances.[35,36] The need for a slow recombination rate was also recognized in studies on the charge generation processes in molecular crystals[37] and on solid−liquid interfaces.[38] The effect of an external field on the special case of diffusion-controlled ion recombination reaction has also been examined within the context of the Noolandi−Hong model.[39]

There exists weakness in these modified Onsager models, as already recognized by Noolandi and Hong themselves.[36] A major problem is that the creation and the recombination of the e−h pairs and their field dependence are not described by rigorous theory. Rather, a somewhat arbitrary form for the rate constant was assumed. For example, in the Noolandi and Hong model, the geminate e−h pair was assumed to return to the first excited state and then relaxes to the ground state with a field-independent rate. The field dependence of the creation rate constant is simply assumed to be an increasing function of the field in such a way it is isotropic at zero field and becoming more peaked in the direction of the field as the field increases.[36] The assumption that the geminate e−h pair recombines to the excited state may hold in a few special cases is certainly not generally applicable. The arbitrarily chosen form of the rate constant and its field dependence are not justified, a weakness already pointed out by the authors themselves.[36] In summary, in spite of the improvement made by these pioneering studies, quantitative treatment of charge generation in polymers on the molecular level is still an elusive goal, one which will be pursued here.

Modern electron transfer theories[40−45] have shown great sucess and can provide a rigorous basis for describing the creation and recombination of a geminate e−h pair. The rate constant is related to the reorganization energy (or the vibrational frequencies of the participating modes) and the free energy change of the electron transfer reaction. The effect of electric field on the rate constant can be modeled through its effect on the free energy change. The well-known Marcus inverted region may provide a theoretical basis for understanding the origin of the slow recombination rate necessary to explain the field-dependent charge generation efficiency in polymers. In spite of the success of Marcus theory in treating electron transfer reactions in solutions and biological systems, it has not been applied to the field-dependent charge generation problem in photoconductive polymers, to the best of our knowledge. As will be shown in this paper, the application of electron transfer theory to low dielectric medium is not trivial and major difficulties have to be solved.

There is another mechanism that can possibly account for the slow recombination rate of the e−h pair. If the precursor for charge generation is a triplet state, then immediately after the electron transfer, the geminate e−h pair still exists as the triplet state. The recombination of triplet e−h pair to the singlet ground state is spin-forbidden and therefore slow. The rephasing from the triplet pair to the singlet pair competes with the hopping motion of the carrier. If the hopping rate is competitive enough againt the rephasing rate, by the time the singlet e−h pair is formed, their separation is far enough to prevent fast recombination. This mechanism can provide a very attractive explanation to the large initial e−h separation distance derived from the Onsager model but apparently has not been discussed in the literature. It is a well-established mechansim operating in CIDNP and magnetic isotope separation experiments.[46,47] This triplet pair mechanism will be considered in this paper.

The organization of this paper is as follows. After the experimentals are described, the spectroscopic properties of fullerene/PVK charge-transfer complexes are first presented (section IIA). This is followed by a detailed characterization of their photoconducting properties, including charge generation and charge transport (sections IIB and IIC). In sections IID and IIE, the magnetic and electric field effects on the charge generation efficiency, the triplet transient absorption, and the singlet fluorescence intensity are presented. The mechanism for charge generation, based on all the experimental data presented, is then proposed in section III. In sections IV and V, we present a theoretical model based on the Onsager and Marcus theory to quantitatively account for the field-dependent charge generation efficiency.

I. Experimental Section

C_{60} and C_{70} were purchased commercially from MER Co. (99.95+% purity). *N*-Poly(vinylcarbazole) (PVK) was purchased from Aldrich (average molecular weight 124000−186000). Thin films of C_{60}- and C_{70}-doped PVK were deposited on aluminum or indium tin oxide (ITO) coated glasses by spin-coating from toluene solutions.

Photoconductivity of the sample was measured by the standard photo-induced discharge method; the details of our experimental conditions have been described before.[49] The sample film is deposited on an electrically grounded aluminum substrate and corona-charged positively or negatively in the dark. Absorption of light generates electrons and holes which migrate to the surface and discharge the surface potential, if the sample is photoconductive. The electrical potential is detected by an electrostatic voltmeter.

The charge generation efficiency, ϕ, is determined from the initial discharge rate of the potential, $(dV/dt)_{t=0}$, under the condition of low light intensity and strong absorption (the

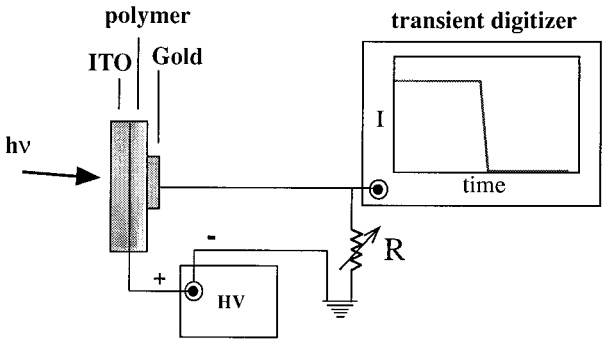

Figure 1. Schematics of the time-of-flight apparatus for the hole mobility measurement.

emission-limited conditions), using the following equation

$$\phi = -\frac{\epsilon}{4\pi eLI}\left(\frac{dV}{dt}\right)_{t=0} \quad (1)$$

where ϵ is the dielectric constant, e the electronic charge, L the film thickness, and I the absorbed photon flux. The incident light intensity was measured with a calibrated radiometer (International Light IL700A). The photon flux at 340 nm used in the current experiments was $\sim 10^{13}$ photons/(cm^2•s), which was essentially all absorbed by the sample at this wavelength. The exposure time is controlled by a Uniblitz shutter, generally limited to 0.3 s or less. The dielectric constant of the film is determined to be 3.2 from capacitance measurement using a HP Model 4194A impedance/gain-phase analyzer.

The mobility of the sample was measured by the conventional time-of-flight method (Figure 1). Fullerene-doped PVK film was deposited onto an ITO glass substrate. A circular thin film gold electrode (in an area of 0.3 cm^2) was then deposited on top of the PVK film to form a sandwiched structure. Electrical leads are attached to the gold and ITO electrodes using silver epoxy. A ~10 ns, 308 nm laser pulse from an excimer laser was used to irradiate the sample from the ITO side. The incident laser energy was kept low, $\leq 36\ \mu$J for a 0.3 cm^2 spot, to ensure that only a small fraction of the surface charges was injected. Carriers were generated near the ITO side of the surface and then drifted toward the gold side under the influence of the applied electric field. The current was detected by an external circuit shown in Figure 1 and digitized by a Tektronix DSA 601A digitizer for data analysis.

The triplet−triplet transient absorption was measured with the flash photolysis apparatus, described in detail before.[9b] The luminescence spectra were taken with a Spex Fluorolog equipped with a cooled R928 photomultiplier tube (250−850 nm). All spectra are corrected for the photodetector response. Low-temperature spectra were taken in either a nitrogen cryostat (Oxford Instruments DN1704) or a continuous flow helium cryostat (Oxford Instruments CF1204). For the electrical field experiments, the sample, fabricated the same way as that in the mobility experiment (Figure 1), is mounted on a sample holder with electrical feedthrough inside the cryostat. The magentic field experiments were performed with permanent magets.

II. Results

IIA. Spectroscopic Properties. Fullerene forms charge-transfer (CT) complex with aromatic electron donors.[4,5] The carbazole group in PVK is an electron donor and is therefore expected to form CT complex with fullerene. The binding constant of the CT complex can be determined[50] by monitoring the absorption spectrum of C_{60} in the presence of *N*-ethylcarbazole (used as a model compound) as shown in Figure 2. Upon

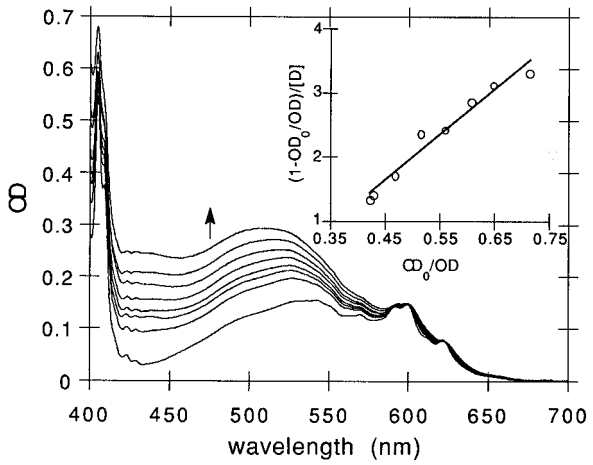

Figure 2. Absorption spectra of C_{60} in methylcyclohexane as a function of increasing concentration (indicated by the arrow) of *N*-ethylcarbazole. The insert shows a plot of $(1 - OD_0/OD)/[\text{carbazole}]$ vs OD_0/OD, where OD is the optical density of C_{60} absorption at 500 nm in the presence of *N*-ethylcarbazole and OD_0 in the absence of *N*-ethylcarbazole. The intercept of the best-fit straight line gives the negative equilibrium constant for C_{60}/*N*-ethylcarbazole charge-transfer complex.

the addition of *N*-ethylcarbazole, a new absorption band appears in the ~450−550 nm region (Figure 2), which is attributed to the C_{60}/ethylcarbazole complex. By plotting $(1 - OD_0/OD)/[\text{ethylcarbazole}]$ vs OD_0/OD, where OD is the optical density of C_{60} in the presence of *N*-ethylcarbazole and OD_0 is the optical density in the absence of *N*-ethylcarbazole, one obtains a straight line. The intercept of the straight line yields $-K$ and the slope yields $(\epsilon_{CT}/\epsilon_f)K$ where K is the binding constant and ϵ_{CT} and ϵ_f are the extinction coefficients of the CT complex and C_{60}, respectively, at the monitoring wavelength.[50] The insert of Figure 2 shows such a plot. The binding constant of C_{60}/*N*-ethylcarbazole charge-transfer complexes at room temperature is thus determined to be 1.5 M^{-1} by this method. The binding constant of C_{70}/*N*-ethylcarbazole is not determined here, but previous work on other electron donors shows both C_{60} and C_{70} CT complexes have similar binding constants.[4,5] The magnitude of the binding constant indicates these are weakly bound CT complexes. Nevertheless, in a PVK film the effective carbazole concentration is very high, about 6 M assuming a homogeneous distribution, and we estimate ~90% of the C_{60} exists as CT complexes. Of course, this value can be somewhat different in a polymer thin film and may be affected by the thin film preparation conditions.

The CT interaction between fullerene and PVK can also be probed by luminescence spectroscopy. Figure 3 shows the room temperature fluorescence spectrum of C_{70} in PVK in comparison with that of C_{70} in methylcyclohexane. Also shown for reference purpose is the 77 K fluorescence spectrum of C_{70}/methylcyclohexane. The sharp vibronic structures of C_{70} fluorescence in methylcyclohaxane merge into a featureless broad band in PVK, with a concurrent red-shift of the fluorescence peak by about 420 cm^{-1} (Figure 3). This is attributed to the CT interaction between C_{70} and PVK and indicates also some structural distortion in the excited singlet state of C_{70}.

Figure 4 shows the phosphorescence spectra of C_{70} in PVK and methylcyclohexane at 77 K. From methylcyclohexane to PVK the phosphorescence spectral peak shifts to higher energy by 254 cm^{-1} with a concurrent broadening of the vibronic structures. Again, this is attributed to the CT interaction between C_{60} and PVK. Because of the very weak luminescence from C_{60},[4] we did not perform these experiments with C_{60} in PVK. However, we expect similar behavior between C_{70} and

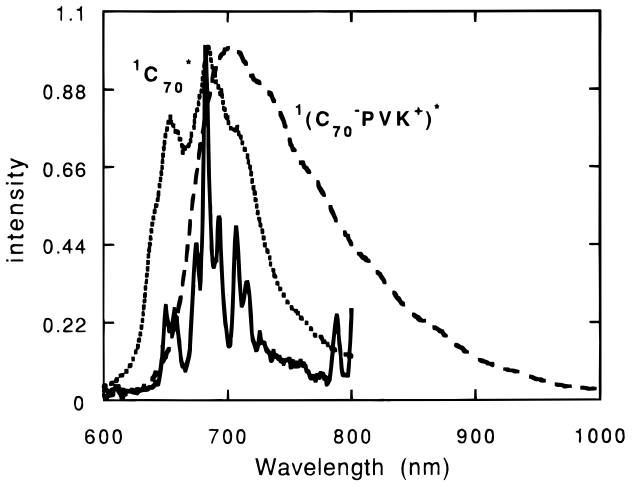

Figure 3. Fluorescence spectra of C_{70} in PVK at room temperature (dashed line) and in methylcyclohexane at room temperature (dotted line) and 77 K (solid line).

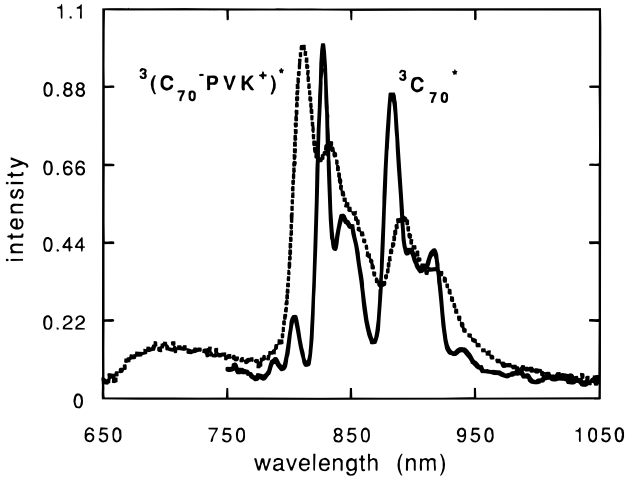

Figure 4. Phosphorescence spectra of C_{70} in PVK (dotted line) and methylcyclohexane (solid line) at 77 K.

C_{70} because of their similar redox potentials[2,3] and binding contants with amines.[4] All these spectroscopic data establish firmly the existence of weakly bounded fullerene/carbazole CT complexes in PVK film which is important for further discussion of the charge generation mechansim.

IIB. Charge transport. Previous studies have established that fullerene-doped PVK and polysilanes are hole-transporting polymers.[17,19] What are the effects of fullerene doping on the hole mobilities of these polymers? The hole mobility can be measured by the time-of-flight method as discussed in the Experimental Section (Figure 1). Electrons and holes are created by a short laser pulse near the surface of the polymer film. Depending on the polarity of the electric field applied on the electrodes, either electrons or holes traverse the bulk of the film. This gives rise to a displacement current which is detected by the external circuitry. Figure 5 shows typical time-of-flight transient curves for fullerene-doped phenylmethylpolysilane and PVK. In the ideal case (nondispersive transport), the current stays constant and falls off to zero at time τ_t, when the charge carriers arrive at the other side of the film. Usually the fall-off near τ_t is smeared out due to spreading of the charge carriers packet, as shown in Figure 5a for C_{70} in phenylmethylpolysilane. The carrier mobility, μ, is determined from the equation $\mu = d/(\tau_t \cdot E)$, where d is the film thickness and E is the applied field.

Carrier transport in polymers is characterized by a succession of hops from site to site. The distances between various

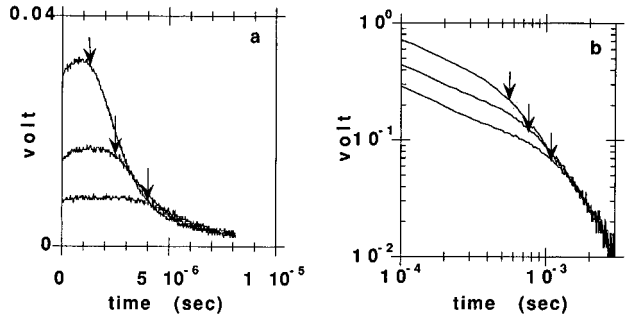

Figure 5. Time-of-flight transient curves for (a) C_{70} in PMPS at 2.5 $\times$ 10^5, 3.1 $\times$ 10^5, and 3.7 $\times$ 10^5 V/cm and (b) PVK at 4.7 $\times$ 10^5, 5.5 $\times$ 10^5, and 6.3 $\times$ 10^5 V/cm. The arrows indicate the approximate location of the transit time, τ_t.

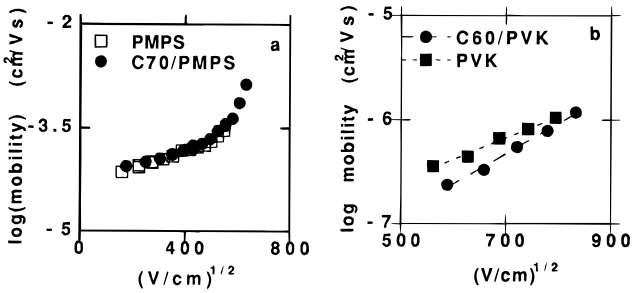

Figure 6. Field-dependent mobility data of (a) 1.6 wt % C_{70}/PMPS vs PMPS and (b) 2 wt % C_{60}/PVK vs PVK.

neighboring sites and the energetics of each site are different. These distributions (dispersions) in energy and distance cause different hopping rates between different sites. This is called dispersive transport, which gives a transient current that deviates from the ideal shape.[51−54] In the extreme case, no discernible break at transit time τ_t can be detected from the time-of-flight curve. This problem was addressed by Scher et al.[51,52] According to the Scher−Montroll model, the dispersive current transient can be analyzed in a double log plot as shown in Figure 5b. The transit time is taken to be the break point in such a log−log plot (Figure 5b).

We have measured the hole mobility of phenylmethylpolysilane (PMPS) and *N*-poly(vinylcarbazole) (PVK) in the absence and presence of fullerenes (Figure 6). PMPS is a σ-conjugated polymer. Extensive delocalization of σ-electrons takes place along the silicon chain, giving rise to very efficient hole transport along the silicon backbone. The hole mobility of polysilanes, $\sim 10^{-4}$ cm^2/(V·s),[55−58] is among the highest observed for polymers. Figure 6a shows the field-dependent hole mobility of PMPS and PMPS doped with 1.6 wt % C_{70}. The presence of C_{70} essentially has no effect on the hole mobility of PMPS. This is presumably because the hole moves along the silicon backbone and is not affected by the small amount of C_{70} present in the surroundings.

In the case of PVK, the polymer backbone does not participate in hole transport directly. Instead, the hole moves by hopping along the pendant groups (i.e. carbazoles). The hole mobilities of this class of polymers are low, around 10^{-6}−10^{-7} cm^2/(V·s).[59] Figure 6b shows the field-dependent hole mobility of PVK and PVK doped with 2 wt % C_{60}. The presence of C_{60} has only a small effect on the hole mobility of PVK. The mobility is slightly lower at low field but has a relatively steeper field dependence for C_{60}/PVK. According to the disorder formalism,[53,54] the high field mobility follows the equation

$$\mu(\hat{\sigma},\Sigma,E) = \mu_0 \exp\left[-\left(\frac{2\hat{\sigma}}{3}\right)^2\right] \exp[C(\hat{\sigma}^2 - \Sigma^2)E^{1/2}] \quad (2)$$

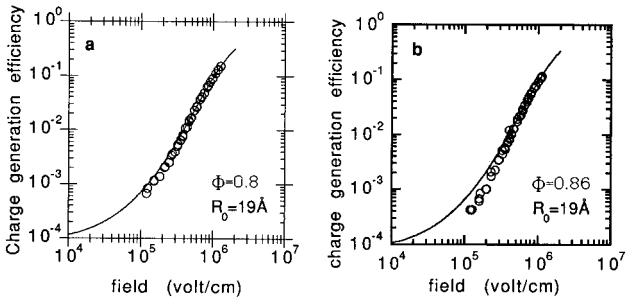

Figure 7. (a) Field-dependent charge generation efficiency of 2.6 wt % C_{60}/PVK at 340 nm, film thickness = 7.1 μm, photon flux = 1.95 $\times$ 10^{13} photons/cm^2. (b) Field-dependent charge generation efficiency of 1.3 wt % C_{70}/PVK at 340 nm, film thickness = 7.8 μm, photon flux = 1.84 $\times$ 10^{13} photons/(cm^2•s).

where $\hat{\sigma} = \sigma/kT$ ($\hat{\sigma}$ is the width of the Gaussian distribution density of states), Σ is a parameter that characterizes the degree of positional disorder, E is the electric field, μ_0 is a prefactor mobility, and C is an empirical constant given as 2.9 $\times$ 10^{-4} (cm/V)$^{1/2}$. In the case of C_{60}/PVK, the smaller intercept and larger slope for the field dependence of hole mobility (Figure 5b) suggest that the introduction of C_{60} increases the positional disorder of PVK slightly, i.e., the distribution width of the distances between carbazole groups becomes wider.

Overall, the effect of a small amount of fullerene dopant on the hole mobility of the polymer is small. It should be noted that this is only true for low concentrations of dopants discussed here. For very high concentration of dopants, especially when the concentration is above the percolation threshold, the transport properties of the polymer can be greatly affected. C_{60} is a known electron conductor. The potential exists for developing electron-transporting polymers based on highly doped C_{60}/polymer.

IIC. Charge Generation. Photoconductivity is the convolution of photoinduced charge generation and charge transport. Since fullerenes have a very small effect on the transport properties of the polymer matrix, their main function is the enhancement of charge generation efficiency. It is of fundamental importance to understand the molecular mechanism by which the charge generation efficiency of the polymer is enhanced in the presence of fullerenes.

The charge generation efficiency of PVK containing a mixture of fullerenes (~85% of C_{60} and ~15% of C_{70}) has been reported by us before.[17,18] Essentially the same results are obtained with pure C_{60}- and C_{70}-doped PVK. Figure 7 shows the field-dependent charge generation efficiencies of C_{60}/PVK (Figure 7a) and C_{70}/PVK (Figure 7b) excited at 340 nm. Low light intensity, ~10^{13} photons/(cm^2•s), was used in these experiments to ensure emission-limited conditions. For example, at 2 $\times$ 10^5 V/cm about 1.5% of the surface charge is discharged by photons within the 0.3 s exposure time. The charge generation efficiency was found to be independent of the sample thickness and strongly field-dependent, with a value of ~0.15 at 10^6 V/cm (Figure 7).[17] The efficiency is higher than that of undoped PVK.[60,61] The ability of fullerene to enhance the photoconductivity of polymers is quite general, as since been shown in several other polymers.[19−22]

The field dependence of the charge generation efficiency can be fitted by the Onsager model.[29,62] The model solves the diffusion equation of the relative motion of an electron−hole pair, bounded by their Coulomb interaction, under an electric field. It predicts the probability that the pair separates into infinity with a given initial separation distance, r_0. An important boundary condition for this model is that if the pair separation distance reaches zero, the pair recombines with an infinitively fast rate. With this assumption, the charge generation efficiency, $\phi(r_0,E)$, in the presence of an electric field, E, is given by[29,62]

$$\phi(r_0,E) = \phi_0\{1 - (2\xi)^{-1}\sum_{j=0}^{\infty} A_j(\eta)A_j(2\xi)\} \quad (3)$$

where

$$\eta = \frac{e^2}{\epsilon kTr_0} \quad (4)$$

$$2\xi = \frac{eEr_0}{kT} \quad (5)$$

and

$$A_{j+1}(\eta) = A_j(\eta) - \frac{\eta^{j+1}e^{-\eta}}{(j+1)!} \quad (6)$$

$$A_0(\eta) = 1 - e^{-\eta} \quad (7)$$

Here ϕ_0 is the quantum yield of the initially generated electron−hole pair. The two parameters, r_0 and ϕ_0, characterize quantitatively the charge generation efficiency of a photoconductor under applied field. For example, a large r_0 value indicates the photoconductor has a large low-field charge generation efficiency while the ϕ_0 value represents the ultimate charge generation efficiency achievable at high field. Figure 7 shows the fit to the Onsager model (solid lines). The ultimate charge generation efficiencies achievable at high field, ϕ_0, are almost quantitative for C_{60} and C_{70} in PVK, being 0.8 and 0.86, respectively. A value of 19 Å for the initial e−h separation distance is required to fit the data (Figure 7). As discussed in the introduction section, this large e−h separation distance is not consistent with the donor−acceptor distance in a charge-transfer complex and is a result of the unrealistic assumption in the the Onsager model. We will present a new and improved model later in section IV of the paper.

IID. Electric and Magnetic Field Effects. It is known that the photoexcited singlet state of C_{60} and C_{70} undergoes efficient intersystem crossing to generate a long-lived triplet state with a quantum yield of almost 1.[25−27] In solutions, where the diffusion of reactants to close distance is required, this long-lived triplet state is therefore expected to be the main species responsible for chemical reactions. In a polymer, however, the reactants lie close to each other such that the short-lived singlet state can react with the neighboring molecules before converting to the triplet state. This is the case for fullerene-doped PVK; both singlet and triplet states can in principle participate in the electron transfer reactions.

If the precursor for charge generation is a triplet state, then immediately after the electron transfer, the geminate e−h pair still exists as the triplet state. The recombination of triplet e−h pair to the singlet ground state is spin-forbidden and therefore slow. The rephasing from the triplet pair to the singlet pair competes with the hopping motion of the carrier. If the hopping rate is competitive against the rephasing rate, by the time the singlet e−h pair is formed, their separation is so far that their recombination rates become very slow. This mechanism can provide a very attractive explanation to the large initial e−h separation distance derived from the Onsager model and the high charge generation efficiency.

Several experimental results, however, can eliminate this triplet mechanism in the case of fullerene-doped PVK. With the triplet e−h pair mechanism one expects to see a magnetic

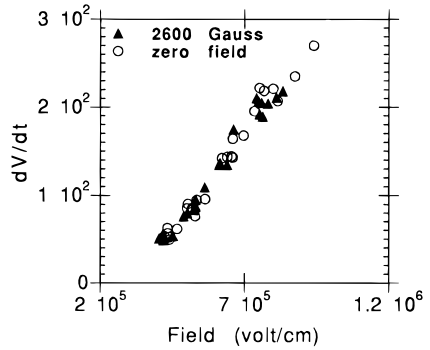

Figure 8. Magnetic field effect on the initial photoinduced discharge rate of 2.6 wt % C_{60}-doped PVK as a function of the applied fields.

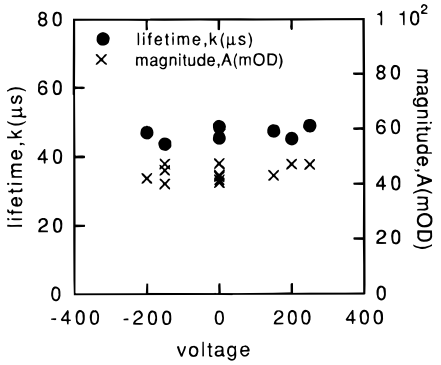

Figure 9. Lifetime and the magnitude (at the end of the laser pulse) of the C_{60} triplet state plotted as a function of the applied fields (both forward and reverse bias). The sample consists of a 3.1 μm thick, 3.6 wt % C_{60}/PVK film sandwiched between an ITO and a gold electrode. The excitation wavelength is 530 nm and the monitoring wavelength is 720 nm.

field effect.[46,47] The charge generation efficiency of fullerene-doped PVK was measured under magnetic fields up to 2600 G, a region that such field effect was expected to occur for a triplet-based mechanism. We did not observe any detectable magnetic field effects (Figure 8).

We have also studied the effects of applied electric fields on the yield and lifetime of the C_{60} triplet state. If the C_{60} triplet state is the precursor for photogenerated carriers, then the lifetime of the triplet state should depend on the applied field and correlate with the field dependence of the charge generation efficiency. We monitor the C_{60} triplet state with the laser flash photolysis technique, discussed in detail before.[9b] In Figure 9, the lifetimes of the C_{60} triplet state are plotted as a function of the applied fields. The absence of any detectable electric field effect up to 5×10^5 V/cm indicates that triplet state is not the precursor of charge carriers. Furthermore, the initial magnitude (at the end of the laser pulse) of the triplet state is also independent of the applied fields. This indicates that part of the fullerene singlet population, which forms the triplet state through the process of intersystem crossing, does not lead to charge carrier generation either. These are presumably fullerenes that do not exist as CT complexes.

The fluorescence intensity of fullerenes, on the other hand, is quenched by the applied electric field. This is shown in Figure 10 for C_{70} in PVK. The field dependence of fluorescence quenching and charge generation efficiency correlate well with each other (Figure 10). Recall that the observed fluorescnece is attributed to the weak CT complexes between C_{70} and PVK (section IIA, Figure 3). This result clearly establishes the singlet state of the CT complex as the precursor for the generation of charge carriers.

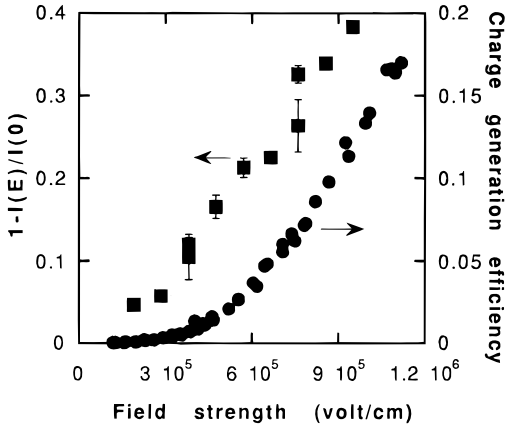

Figure 10. Effects of applied field on the C_{70} fluorescence intensity, excited at 500 nm (■) and charge generation efficiency (●) of C_{70} in PVK.

SCHEME 1

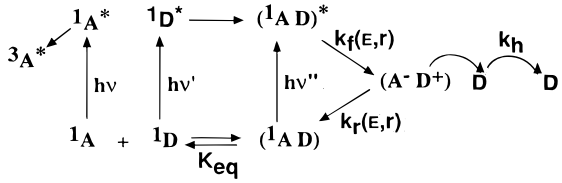

III. Proposed Charge Generation Mechanism

All the data presented in the previous section points to a singlet-based mechanism. Furthermore, since ~90% of the fullerene exists as weak CT complexes in PVK as estimated from the known binding constant (section IIA), the photoexcitation of these CT complexes therefore has to contribute to the photoconductivity in its absorption band region (it is possible for impurity contribution outside of the absorption band of fullerene CT complex). The direct excitation of a small percentage of uncomplexed fullerene does not lead to charge generation as shown by the laser flash photolysis data. The excitation of uncomplexed carbazole moieties can lead to excited state complex formation by energy transfer. The mechanism of charge carrier generation in fullerene-doped PVK is therefore proposed as shown in Scheme 1. In Scheme 1 A, D, and (^{1}A D) represent fullerene, donor (i.e., carbazole), and their charge-transfer complex, respectively. K_f, k_r, and k_h are the forward electron transfer rate constant, the recombination rate constant, and the hole-hopping rate constant, respectively. The hole-hopping rate, $1/k_h$, competes with the electron−hole recombination rate, $1/k_r$. All of the rate constants can be field- and distance-dependent. In the rest of this paper, we will try to provide a quantitative solution to this model and compare to the experimental data.

As discussed before, fitting of the experimental data with the Onsager model yields a large initial electron−hole separation distance of 19−27 Å for fullerene-doped PVK[17] and polysilane,[19a] which is in apparent contradiction with the fact that an electron−hole pair generated from a singlet charge-transfer complex should be separated by only a few angstroms for contact CT complex and <10 Å for solvent-separated CT complex. This paradox is a well-known problem of the Onsager model[29] when applied to polymeric photoconductors,[34] recognized for many years by Braun[35] and Noolandi and Hong.[36] Any succesful new model has to be able to address this paradox.

The boundary condition used in the Onsager model corresponds to the assumption that when the separation distance of an electron−hole pair reaches zero, it recombines with an

infinitely fast rate. This assumption is unrealistic in the real system. For an electron−hole pair to recombine to the ground state, several electronvolts of energy have to be disposed of, usually dumped into the vibrational modes of the system. This can be a slow (∼nanoseconds) process because of the large amount of energy involved. Next, the creation and recombination rate may depend on the field, separation distance, and energetics. None of these is considered by the Onsager model.

Both Braun[35] and Noolandi and Hong[36] have attempted to remedy the need for a finite recombination rate in the Onsager model. Braun suggested a model which identifies the geminate electron−hole with the excited charge-transfer state, which typically has a lifetime on the scale of nanoseconds.[35] Noolandi and Hong[36] solves for the escape probability of an electron−hole pair using a different boundary condition than the original Onsager model. Their boundary condition corresponds to a finite surface recombination velocity on a partly absorbing sphere of finite radius. Indeed, by assuming a slow recombination rate (taken to be the lifetime of either the charge transfer state or the singlet state), the field dependence data can be fitted by these modified Onsager models with small initial e−h separation distance.[35,36] However, in these models there was no explanation for the origin of the slow recombination rate and the electric field dependence is not considered. Furthermore, there is no theory for either the creation or the escape rate of the electron−hole pair. Rather, a somewhat arbitrary form for the escape rate was assumed, a weakness already recognized by Noolandi and Hong.[36] In summary, in spite of the improvement made by these pioneering studies, quantitative treatment of charge generation in polymers on the molecular level is still an elusive goal. In the next section, we attempt to address this problem.

IV. Theoretical Modeling

We have developed a model to analyze field-dependent charge generation in low dielectric medium. The model incorporates the Marcus electron transfer theory[40,41] to describe the creation and recombination of e−h pairs and an Onsager-like model to treat charge diffusion under electrical field. In spite of the success of the Marcus electron transfer theory in treating electron transfer reactions in polar media, to the best of our knowledge it has not been applied to study the photoconductivity of polymers. The main difficulty is that in low dielectric constant media, the Coulomb interaction between e−h pairs is not negligible. As a result, the free energy change (ΔG) and the electron transfer rate constant are distance-dependent. This distance dependence of ΔG is usually ignored in treating electron transfer reactions in polar media.[40,41] To the best of our knowledge, this is the first attemp to address the problem of charge separation in polymers.

In the following we first discuss the formalism of the model and then a numerical solution to the problem.

IVA. Diffusion of Charge Pair. We describe the diffusion of a charge pair in a continuous, isotropic medium in terms of the pair distribution function $\rho(\mathbf{r})$ giving the probability density for finding a hole within a volume element d^3r at a location displaced from the position of an electron by the vector $\mathbf{r} = (x, y, z)$. The diffusion constant D is the sum of the diffusion constants of electron and hole. The electric mobility μ, the sum of electron and hole mobilities, is related to D via the Einstein relation $D = kT\mu/e$, where e is the electronic charge. We use cgs units here. The current describing the separation of hole and electron is given by

$$\mathbf{j}(\mathbf{r}) = -\mathrm{D}\,\nabla\rho(\mathbf{r}) + \mu\,\mathbf{E}(\mathbf{r})\,\rho(\mathbf{r})$$

$$= -\mathrm{D}\left(\nabla\rho(\mathbf{r}) + \frac{e}{kT}\nabla V(\mathbf{r})\,\rho(\mathbf{r})\right) \quad (8)$$

$$\equiv -D(\nabla\rho(\mathbf{r}) + \nabla W(\mathbf{r})\,\rho(\mathbf{r}))$$

Here we have introduced the electric field $\mathbf{E}(\mathbf{r})$, assumed to depend only on the electron−hole separation $\mathbf{r}$, and the associated potential $V(\mathbf{r})$, in dimensionless form $W(\mathbf{r}) = eV(\mathbf{r})/(kT)$. For the present problem

$$V(\mathbf{r}) = -\frac{e}{\epsilon \boldsymbol{r}} - E_0 z \quad (9)$$

where ϵ is the static dielectric constant of the medium, and the z-direction has been chosen as pointing from the electron to the hole in the direction of the external field, of magnitude E_0. Conservation of particles leads to the following steady-state transport equation for the pair distribution function

$$\nabla\cdot\mathbf{j}(\mathbf{r}) - \beta(\mathbf{r})\,\rho(\mathbf{r}) = s(\mathbf{r}) \quad (10)$$

Here, $\beta(\mathbf{r})$ is the rate constant describing electron−hole annihilation at a separation $\mathbf{r}$, while $s(\mathbf{r})$ gives the rate of pair creation at this separation and is proportional to s_0, the rate of production of singlet excited states by photons. These quantities are here presented as derived from the Marcus theory of electron-transfer reactions.

After (10) is solved with appropriate boundary conditions, the photogeneration efficiency is obtained as the ratio of the flux escaping to infinity to the singlet production rate

$$\text{efficiency} = \frac{1}{s_0}\int_S \mathrm{d}^2 r\;\mathbf{j}(r)\cdot\mathbf{n} \quad (11)$$

where the surface integral ($\mathbf{n}$ is the normal to the surface) is on a surface S such that all creation and annihilation takes place inside S.

IVB. Marcus Electron Transfer Theory. The theory of Marcus as we apply it here gives the rate of a charge-transfer reaction in the form[40,41]

$$k_{\mathrm{M}} = \nu \exp\left[-\frac{(E_{\mathrm{f}} - E_{\mathrm{i}} + \lambda)^2}{4\lambda k_{\mathrm{B}} T}\right] \quad (12)$$

Here, E_{i} and E_{f} are the energies of the initial and final states, and λ, called the reorganization energy, is a phenomenological parameter describing the collective effects of the vibronic interactions in the initial and final states. The prefactor ν involves wave function overlap integrals and is phenomenologically characterized as depending on the charge separation distance r via

$$\nu(r) = \nu_0 \exp[-\alpha(r - r_0)] \quad (13)$$

The prefactor ν_0 tends to be universally about 10^{13} s^{-1} when r_0, the minimum charge separation distance, has its lowest physically allowed value (i.e., without any external constraints).

Expression 12 is exact for the case of a single vibronic level having the same vibrational frequency in the initial and final states. The reorganization energy λ is then the shift in the vibrational energy resulting from the displacement of the energy minimum between the initial and final vibronic states. This notion is illustrated in Figure 11, as we have applied it to describe the photogeneration and annihilation of charge pairs.

As indicated in Figure 11, we take the singlet excited state as vertically displaced from the single parabolic vibronic ground state, while the charge transfer state is both vertically and

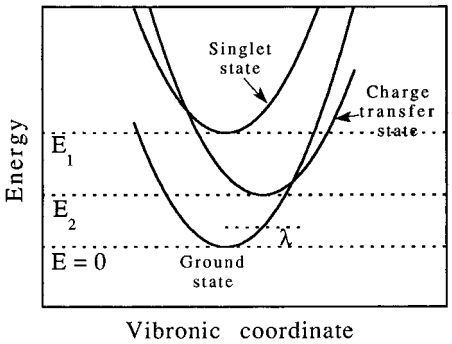

Figure 11. Schematic of Marcus theory applied to pair creation and annihilation (see text).

horizontally displaced. Thus if the dominant vibronic coordinate is a bond length, we assume this bond length does not change substantially upon excitation to the singlet excited state but does change when this state dissociates to form the charge transfer state. Pair generation is viewed here as a transition from the singlet to the charge transfer state; annihilation occurs when the charge transfer state collapses back to the ground state. In the scheme shown, creation and annihilation are characterized by the same reorganization energy λ in the Marcus phenomenology; only the initial and final energies in expression 12 are different for these two processes.

A critical feature of our theory is that the electronic energy of the charge transfer state depends on both the electron−hole separation and the external electric field

$$E_2 = E_2^{\infty} - \frac{e^2}{\epsilon r} - E_0 z \tag{14}$$

where E_2^{∞} is the energy of the charge transfer state in the absence of an external field and with infinite separation of electron and hole.

We can now write down explicit expressions for the annihilation and creation parameters $\beta(\mathbf{r})$ and $s(\mathbf{r})$. The annihilation parameter is just the recombination rate:

$$\beta(\mathbf{r}) = \nu_0 \exp\left[-\alpha(r - r_0) - \frac{\left(-E_2^{\infty} + \frac{e^2}{\epsilon r} + E_0 z + \lambda\right)^2}{4\lambda k_B T}\right] \tag{15}$$

The rate of creation of charge transfer pairs depends on the density of available donor molecules ρ_d and is in competition with the nonradiative decay of the singlet excited state directly to the ground state, at a rate k_s. We assume a uniform density for these donor molecules; i.e., there is no correlation between the location of donor and acceptor molecules. The singlet decay competes with the *total* rate of CT pair production, and the rate of production of CT pairs per unit volume can be expressed as

$$s(\mathbf{r}) = \frac{s_0\, k_{ct}(\mathbf{r})}{k_s + \int_{r \geq r_0} \rho_d\, k_{ct}(\mathbf{r})\, d^3 r} \tag{16}$$

where

$$k_{ct}(\mathbf{r}) = \nu_0 \exp\left[-\alpha(r - r_0) - \frac{\left(E_2^{\infty} - \frac{e^2}{\epsilon r} - E_0 z - E_1 + \lambda\right)^2}{4\lambda k_B T}\right]$$

The singlet production rate s_0 appearing in (16) cancels in the expression for the efficiency, eq 11.

We will solve for the general case of an electron transfer reaction from the surrounding donors to the fullerene, where the electron is assumed to be trapped somewhere on a spherical surface representing the fullerene. Only the hole is mobile and is created according to eq 16. The simpler case of charge between two points in a uniform medium can be obtained from this program simply by setting the fullerene radius to zero.

When the fullerene radius is not zero and the external field is finite, one has to properly average over all positions of the trapped electron. The way this was done was to assume that donor molecules are uniformly distributed around the fullerene, at a distance r_0 beyond the fullerene radius (r_0 is the minimum electron−hole separation in (13)); the trapped electrons, however, will not be uniformly distributed, since any given donor molecule will tend to put an electron wherever the charge transfer rate $k_{ct}(\mathbf{r})$ is greatest on the fullerene surface ($\mathbf{r}$ is the relative donor-electron position vector).

The efficiency has to be calculated for each position of the trapped electron before averaging; i.e., the problem to be solved contains a single trapped electron only. For any one such position, except a polar one, the problem does not possess axial symmetry and one is confronted with a full-blown three-dimensional diffusion problem.

V. Numerical Solutions

VA. Virtual Lattice Approximation of Diffusion. The numerical solution of (10) over a three-dimensional grid, including the boundary condition that ρ must approach zero at infinite distances, presents enormous difficulties. The grid must be fine enough to contain details of the variation of the creation and annihilation rates and must expand at larger separations of r. The number of points on this grid must, of course, be finite. If we also wish to make the grid fine enough to permit finite difference approximations to the differential operators, the problem becomes intractable in practice.

We have appealed to physical reasoning to construct a rather coarse grid which satisfies the first two requirements only, on a finite-sized grid. In the absence of sources and sinks, eq 10 is solved by the equilibrium distribution

$$\rho_{eq}(\mathbf{r}) = \rho_0 \exp\left[-\frac{-\frac{e^2}{\epsilon r} - E_0 z}{k_B T}\right] \tag{17}$$

and the current is identically zero. The numerical model must correctly describe the tendency to approach this equilibrium distribution, as modified by sources and sinks.

We imagine that the hole moves on a virtual lattice, each lattice site representing a volume element located at a grid point. Let $p(\mathbf{r}_1)$ be the probability of occupation of the site at $\mathbf{r}_1$ and $k(\mathbf{r}_1,\mathbf{r}_2)$ the rate constant describing the transition rate to the site at $\mathbf{r}_2$ as $k(\mathbf{r}_1,\mathbf{r}_2)\, p(\mathbf{r}_1)$. Let $v(\mathbf{r}_1)$ be the volume of the volume element at $\mathbf{r}_1$. Equation 17 then requires

$$k(\mathbf{r}_1,\mathbf{r}_2) = k(\mathbf{r}_2,\mathbf{r}_1)\, \frac{v(\mathbf{r}_2)}{v(\mathbf{r}_1)} \exp[-W(\mathbf{r}_2) + W(\mathbf{r}_1)] \tag{18}$$

where

$$W(\mathbf{r}) \equiv \frac{-\frac{e^2}{\epsilon r} - eE_0 z}{k_B T}$$

These transition rate constants completely characterize the diffusion process, since creation and annihilation events involve

only single grid points. The transition rate constants $k(\mathbf{r}_1,\mathbf{r}_2)$ must be chosen such that the correct transport equation is reproduced in the limit of an infinitely fine mesh. It turns out that this limit is reached most rapidly if the ratio of rate constants in (18) is distributed symmetrically between $k(\mathbf{r}_1,\mathbf{r}_2)$ and $k(\mathbf{r}_2,\mathbf{r}_1)$, and we obtain

$$k(\mathbf{r}_1,\mathbf{r}_2) = \frac{D}{|\mathbf{r}_1 - \mathbf{r}_2|^2}\sqrt{\frac{v(\mathbf{r}_2)}{v(\mathbf{r}_1)}}\exp\left[-\frac{1}{2}(W(\mathbf{r}_2) - W(\mathbf{r}_1))\right] \quad (19)$$

Equation 10 now takes on the simple form of a set of linear equations for the occupation probabilities $p(\mathbf{r}_i)$ for the cell at $\mathbf{r}_i$

$$-p(\mathbf{r}_i)\sum_j k(\mathbf{r}_i,\mathbf{r}_j) + \sum_j p(\mathbf{r}_j)\,k(\mathbf{r}_j,\mathbf{r}_i) - \beta(\mathbf{r}_i)\,p(\mathbf{r}_i) = s(\mathbf{r}_i)\,v(\mathbf{r}_i) \quad (20)$$

The boundary conditions on (10) appear in (20) as follows:

(a) There are no cells with $|\mathbf{r}_i| < r_{\min} = r_B + r_0$, where r_B is the fullerene radius.

(b) The condition at infinity means that the outermost cells have additional rates of loss corresponding to flux of holes escaping to infinity. The total such flux, relative to the total source flux, determines the efficiency. Since we cannot meaningfully set $\mathbf{r}_2$ equal to infinity in (19), this flux to infinity was handled by postulating another layer of cells, just beyond the outermost cells, whose occupation probability does not enter into (20) but is assumed zero.

Unfortunately, it turns out that the numerical solution of (20) is beset with great inherent difficulties for typical values of the theoretical parameters.

VB. Numerical Difficulties. The basic source of numerical difficulties in this problem is the fact that in the physical space spanned by the problem electrostatic energies vary by many times the thermal energy k_BT. Thus, for $\epsilon = 3$ and a minimum electron−hole separation $r_0 = 5$ Å the room-temperature value of $e^2/(\epsilon r_0 k_B T)$ is 37.1; even in the absence of an external field, equilibrium densities will vary by as much as a factor $\exp(37.1) = 1.3 \times 10^{16}$ between r_0 and infinity. But efficiencies are computed by calculating the flux at infinity resulting from sources near r_0. For the linear problem (20), it would appear that a numerical accuracy well in excess of 16 digits is required for a meaningful solution.

As a concrete illustration of this difficulty, consider the following analytically solvable problem (the zero-field Onsager case): We suppose that, with zero external field, creation takes place at a distance r_1 only, while annihilation takes place at an infinite rate at $r = r_0$. The solution for $\rho(r)$ has the form

$$\rho(r) = c(e^{e^2/(\epsilon rkT)} - 1) \qquad \text{for } r \geq r_1$$

$$= c'(e^{e^2/(\epsilon r_0 kT)} - e^{e^2/(\epsilon rkT)}) \qquad \text{for } r_0 \leq r \leq r_1 \quad (21)$$

where c'/c is determined from the continuity of $\rho(r)$ at $r = r_1$. Since the equilibrium distribution $\exp[e^2/(\epsilon rkT)]$ has no current, the current needed to compute the efficiency comes from the constant term (independent of r) in (21). This constant term must not be neglected numerically in the total density, even though it may be extremely small compared to the equilibrium term. In this example, $\exp[e^2/(\epsilon r_1 kT)]$ must not overwhelm 1 and in turn must not be overwhelmed by $\exp[e^2/(\epsilon r_0 kT)]$.

The difficulty just discussed leads to a lower limit on the value of the minimum electron−hole separation r_0, depending on the numerical accuracy of the computation. Another difficulty arises when finite fields are present. Then the equilibrium distribution diverges at *large* distances, leading to a similar limitation on the maximum electron−hole separation, but one that depends on the particular value of the field. The physics of the problem is correctly modeled provided the hole is permitted to go sufficiently far so that the field of the electron is negligible compared to the external field. The critical radius r_c, where these two fields balance, is given by

$$r_c = \sqrt{\frac{e}{\epsilon E}} \quad (22)$$

The maximum radius of the finite-mesh virtual lattice must be greater than r_c yet not be so large that $\exp[E_0 r_c/(kT)]$ numerically overwhelms $\exp[E_0 r_0/(kT)]$. The effect of this constraint is to limit the maximum value of the external field for which the photogeneration efficiency can be computed to a value which depends on the computational accuracy.

A useful way of thinking about these limitations is in terms of the characteristic dimension sometimes called the Onsager radius, $r_{Ons} = e^2/(\epsilon kT)$, whose room-temperature value for $\epsilon = 3$ is 185 Å. The minimum distance r_0 must not be so small that the ratio r_{Ons}/r_0 exceeds the logarithm of the largest sustainable numerical ratio. The natural unit of field consists of a voltage drop of $(kT)/e$ (0.025 V at room temperature) across one Onsager radius, about 1.5×10^4 V/cm. The applied field must not exceed this unit by a factor equal to the same logarithm. For example in a 14-digit (VAX double precision or CRAY single precision) calculation, it is difficult to maintain a final accuracy much better than 10 digits, when this logarithm [$\ln(10^{10})$] is about 23. Such an accuracy leads us to suspect numerical results in this problem whenever r_0 is less than about 8 Å or when E_0 exceeds about 5×10^5 V/cm. A CRAY double-precision calculation (28 digits intrinsic) can extend these limits to about 3.5 Å and 10^6 V/cm.

In practice we found that the calculation fails if r_{max}, the maximum electron−hole separation in our finite mesh, is such that $E_0\, r_{max}/(kT)$ is too large, and we found it necessary to restrict this ratio to 10. With this restriction, r_{max} becomes comparable to r_c, eq 22, when E_0 is about 1.3×10^6 V/cm (for $\epsilon = 3$).

The dilemma one now faces is the fact that the numerical accuracy of the final result degrades as we try to improve its physical accuracy by going to a finer mesh, and a compromise must be struck. We have attempted to minimize the number of numerical manipulations by techniques described below as well as to introduce some error correction by appealing to a rigorous conservation law.

VC. Method of Solution. For N cells of the mesh, eq 20 represents an N by N matrix equation. The mesh was drawn on a spherical coordinate system. We chose as a minimally adequate angular mesh one consisting of 10 divisions of the polar angle θ (representing equal divisions of $\cos(\theta)$) and of 6 divisions of the azimuthal angle ϕ, spanning π (mirror symmetry allows us to look at only half the range). With polar cells not divided by the ϕ mesh, this leads to a total of $N_a = 65$ angular mesh points. Then even a minimal radial mesh of $N_r = 20$ points would lead to $N = 1300$; not only is such an N by N matrix difficult to solve by standard routines, but the resultant cumulative errors are expected to be entirely unacceptable in view of the discussion in the previous section. Instead, we made use of the fact that the matrix in question is rather sparse, connecting only nearest neighbor cells, to turn (20) into a system of N_r matrix equations involving matrices of degree N_a by N_a. In this way N_r can be specified at run time and the r-mesh readily varied to obtain an optimal value. Each equation represents the interaction of cells within a given radial shell and the two neighboring radial shells. The solution is propagated from shell to shell between the largest and smallest radii; the boundary

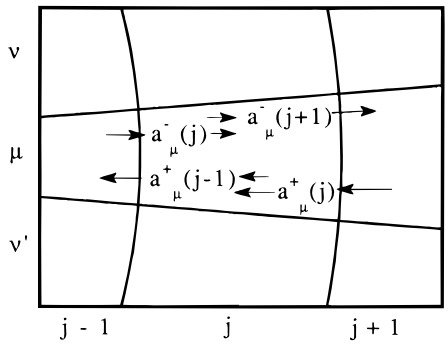

Figure 12. Intershell matrix elements. Radial shells are labeled in the horizontal direction and angular cells in the vertical.

condition at the final extreme results in a single N_a by N_a matrix equation. The procedure is spelled out in detail in the following.

We work in N_a dimensional space, using the convention that capital letters denote N_a by N_a matrices, lower case letters vectors of length N_a. We label these quantities by a label j in parantheses, where j numbers the r-shells, choosing $j = 1$ at the outermost shell. Thus $p(\mathbf{r}_i)$ of eq 20 becomes $p(j)$, and $s(\mathbf{r}_i)$ $v(\mathbf{r}_i)$ will be written for short as $s(j)$. The matrix connecting the occupation probabilities in (20) will be denoted by $A(j)$ for elements within the same shell, while intershell matrix elements, which join identical angle cells between adjacent radial shells, will be denoted by $a^+(j)$ and $a^-(j)$, where $a^{\pm}(j)$ represents a transition into the jth shell from the $(j \pm 1)$th shell (see Figure 12).

Let us define the vector c whose components equal the net radial current passing from a given angular cell of the jth shell to the same angular cell in the $(j + 1)$th cell

$$c_\mu(j) \equiv a_\mu^-(j+1)\, p_\mu(j) - a_\mu^+(j)\, p_\mu(j+1) \qquad (23)$$

Equation 20 takes on the form

$$\sum A_{\mu\nu}(j)\, p_\nu(j) + c_\mu(j-1) - c_\mu(j) = s_\mu(j) \qquad (24)$$

Equations 23 and 24 can be rewritten as recursion relations for $p(j)$ and $c(j)$

$$p_\mu(j+1) = \frac{1}{a_\mu^+(j)}[a_\mu^-(j+1)\, p_\mu(j) - c_\mu(j)]$$

$$c_\mu(j+1) = \sum A_{\mu\nu}(j+1)\, p_\nu(j+1) + c_\mu(j) - s_\mu(j+1) \quad (25)$$

These can be solved iteratively, beginning with $p(1) = 0$ (outermost shell is unoccupied) and $c(1)$ treated as an unknown vector. The result is an expression for $c(N_r)$ as a function of $c(1)$. Setting $c(N_r) = 0$ (there is no current flowing inward from the innermost shell) yields an equation for $c(1)$, the unknown inward current from the outermost shell, i.e., the negative of the current flowing out to infinity. This current is needed in expression 11 for the efficiency, now taking the form

$$\text{efficiency} = -\frac{1}{s_0}\sum_\mu c_\mu(1) \qquad (26)$$

In practice it was found that it was better to carry out the above procedure by transforming eqs 25 to a basis such that one of the N_a components of the transformed current vector is the total current. This is the only component needed in expression 26 for the efficiency. This was done by essentially selecting the vector $e_1 = (1,1,1,1, ...)$ as one of the basis vectors, the remainder an arbitrarily selected set of mutually orthogonal vectors orthogonal to e_1.

In the absence of annihilation or creation, the total current must be the same for each radial shell. Knowledge of this fact allowed us to perform at least a partial error correction at each step of the iteration, avoiding cumulative round-off errors in at least this, the most important component of the transformed current vector. The efficacy of this trick could be demonstrated by comparing single-precision CRAY (14 digit) evaluations, for cases expected to be marginally accurate, with double-precision CRAY (28 digit) calculations. In single precision, the system of linear equations for $c(1)$ was for such cases often found "ill-conditioned" by the library routine employed and, in fact, resulted in a solution which did not satisfy the original set of equations, except for the one critical component of the current. Nevertheless, the corresponding double-precision evaluation, for which the solution of the system of equations was well-behaved, gave essentially the same result for this component.

After $c(1)$ is found, a self-consistency check can be performed by repeating the iteration (25), now beginning with the known $c(1)$. This yields the occupation probabilities $p_\mu(j)$ and lets us evaluate the annihilation rate explicitly. The total rate of loss via annihilation plus the total flux escaping to infinity must add up to the total creation rate:

$$\sum_{j,\mu}\beta_\mu(j)\, p_\mu(j) - \sum_\mu c_\mu(1) = \sum_{j,\mu} s_\mu(j) \qquad (27)$$

Any discrepancy between the calculated values of the left and right hand sides of (27) gives an error estimate for the calculation.

VI. Comparison with Experiments

We have performed the numerical calculation on a Cray C94/4128 computer. As mentioned above, the program has to be run in double precision and typically takes $\sim 4 \times 10^4$ s of CPU time for a 10 point field-dependent calculation. For the case of fullerene in PVK, all necessary parameters are known and the only unknowns are the reorganization energy, λ, and the minimum e−h separation distance, r_0. Parameters used in the calculation are listed below. Fullerene radius is taken to be 3.6 Å. Dielectric constant of the film is measured to be 3.2. Hole diffusion constant in PVK was taken to be 0.0077 cm^2/s.[63] The Marcus prefactor ν_0 is taken universally to be 10^{13} s^{-1} and the α parameter is taken to be 1.5.[40] The average separation distance of donors (i.e., carbazole) is calculated to be 6.4 Å.[28] The energy of the singlet state, E_1, of C_{60} is 1.9 eV with a decay rate constant of 1.6×10^9 s^{-1}.[5] The energy of the charge transfer state in the absence of an external field and with infinite separation of electron and hole, E_2^∞, is 1.53 eV based on the known redox potentials of C_{60} and PVK.[9] Small variation of these numbers (due to experimental uncertainties) is not very important as the calculation is much more sensitive to the values of λ and r_0. In all the calculations an r-interval of 20 is sufficient to achieve convergence.

Figure 13 shows the comparison of theory to the experimental results of photoinduced charge generation efficiency of C_{60}-doped PVK. The data can be fitted quite well using $\lambda = 0.64$ eV and $r_0 = 6.65$ Å. The minimal separation distance of 6.65 Å is defined as from the edge of the C_{60} to the center of the donor, therefore a reasonable distance for a contact CT complex. The 0.64 eV reorganizational energy also falls in the commonly observed range for electron transfer reactions. This demonstrates that field-dependent electron transfer processes in nonpolar medium can now be described quantitatively on the

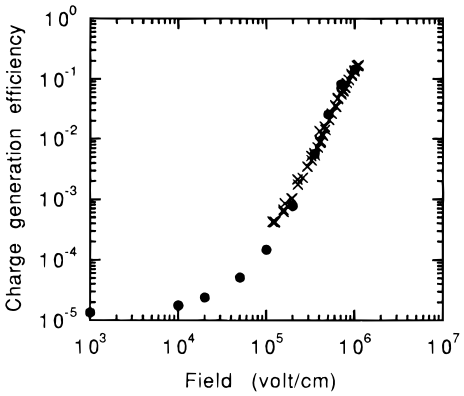

Figure 13. Comparison of experimental values (×) of the charge generation efficiency of C_{60}/PVK with theoretical calculation (●). The best-fit parameters are given in the text.

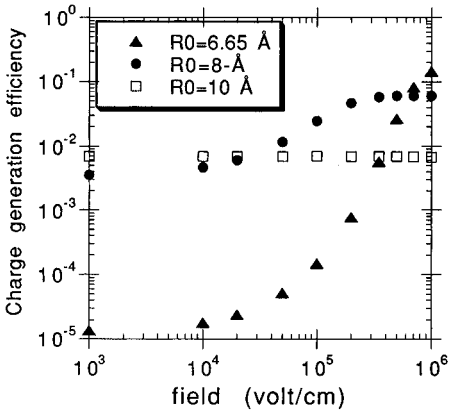

Figure 14. Calculated field dependence of the charge generation efficiency as a function of the separation distance between C_{60} and carbazole. The parameters used are the same as those used in Figure 13.

molecular level within the framework of the theoretical model developed here.

Several possibilities exist to further refine this model in the future. First, a more sophisticated version of the electron transfer theory may be used.[40−45] These refined theories require the inclusion of additional parameters such as an electron−phonon coupling parameter, phonon frequencies, etc. in the model. Secondly, different reorganization energies for forward and backward electron transfer reactions may be used. In the present model, they are assumed to be the same. It is also possible to determine the reorganization energies experimentally by studying a series of fullerene electron transfer reactions with varying donor oxidation potentials and/or fullerene reduction potentials. This will eliminate one or two fitting parameters.

In its present form, this model is useful as a predictive tool for the design of better photoconductors. Because of the complex dependence of reaction rates on the distances and energetics for electron transfer processes in nonpolar media, such predictive ability has been lacking. Much insight can be gained from these calculations, and the results are not always intuitively obvious. One illustrative example is given below.

We calculated the field-dependent charge generation efficiency between C_{60} and carbazole as a function of their separation distances in a medium with a dielectric constant of 3.2. All of the parameters are the same as those used to fit the data in Figure 13. The computational results are shown in Figure 14. Because of the use of the classical Marcus electron transfer theory which gives an unrealistically steep dependence of the reaction rate on the energetics, the results should not be used quantitatively but only as a tool for identifying trends.

For this particular reaction, the initial increase of the separation distance results in an *increase* of the charge separation efficiency. Further increase of the separation distance results in a flat field depencence and lower charge generation efficiency (Figure 14). These results are certainly not obvious and are unique for low dielectric constant media. For high dielectric constant media, the calculation shows a decrease of the charge generation efficiency with increasing distance, as expected intuitively. These results therefore suggest that better fullerene-based polymer photoconductors may be obtained by optimizing the separation distance between the C_{60} and the donor. This may be achieved by using C_{60} attached with a side chain of variable length or encapsulated in another molecule such as cyclodextrin. These interesting predictions remain to be confirmed experimentally in the future.

Acknowledgment. We wish to thank Dr. Jon Caspar for his assistance in taking the laser flash photolysis data and Ms. Sarah Harvey for technical assistance.

References and Notes

(1) Kratschmer, W.; Lamb, L. D.; Fostiropoulos, K.; Huffman, D. R. *Nature* **1990**, *347*, 354−358.
(2) Haufler, R. E.; Conceicao, J.; Chibante, P. F.; Chai, Y.; Byrne, N. E.; Flanagan, S.; Haley, M. M.; O'Brien, S. C.; Pan, C.; Xiao, Z.; Billups, W. E.; Ciufolini, M. A.; Hauge, R. H.; Margrave, J. L.; Wilson, L. J.; Curl, R. F.; Smalley, R. E. *J. Phys. Chem.* **1990**, *94*, 8634.
(3) Allemand, P. M.; Koch, A.; Wudl, F.; Rubin, Y.; Diederich, F.; Alvarez, M. M.; Anz, S. J.; Whetten, R. L. *J. Am. Chem. Soc.* **1991**, *113*, 1050.
(4) Wang, Y. *J. Phys. Chem*. **1992**, *96*, 1530.
(5) Sension, R. J.; Szarka, A. Z.; Smith, G. R.; Hochstrasser, R. M. *Chem. Phys. Lett.* **1991**, *185*, 179.
(6) Allemand, P.-M.; et al. *Science* **1991**, *253*, 301.
(7) Wang, Y.; Cheng, L.-T. *J. Phys. Chem*. **1992**, *96*, 764.
(8) Arbogast, J. W.; Foote, C. S.; Kao, M. *J. Am. Chem. Soc*. **1992**, *114*, 2277.
(9) (a) Wang, Y.; Herron, N.; Caspar, J. V. *Mater. Sci. Eng.* **1993**, *B19*, 61. (b) Caspar, J. V.; Wang, Y. *Chem. Phys. Lett.* **1994**, *218*, 221.
(10) Watanabe, A.; Ito, O. *J. Chem. Soc., Chem. Commun*. **1994**, 1285.
(11) Sun, Y. P.; Bunker, C. E.; Ma, B. *J. Am. Chem. Soc*. **1994**, *116*, 9692.
(12) (a) Kamat, P. V. *J. Am. Chem. Soc.* **1991**, *113*, 9705. (b) Sauve, G.; Dimitrijevic, N. M.; Kamat, P. V. *J. Phys. Chem*. **1995**, *99*, 1199.
(13) Hwang, C. K.; Mauzerall, D. *Nature* **1993**, *361*, 138.
(14) Sariciftci, N. S.; Smilowitz, L.; Heeger, A. J.; Wudl, F. *Science* **1992**, *258*, 1474.
(15) Grzeskowiak, K. N.; Smirnov, S. N.; Braun, C. L. *J. Phys. Chem*. **1994**, *98*, 5661.
(16) Williams, R. M.; Verhoeven, J. W. *Chem. Phys. Lett.* **1992**, *194*, 446.
(17) Wang, Y. *Nature* **1992**, *356*, 585.
(18) Wang, Y. U.S. Patent 5,250,378, Oct 5, 1993.
(19) (a) Wang, Y.; West, R.; Yuan, C. H. *J. Am. Chem. Soc.* **1993**, *115*, 3844. (b) Kepler, R. G.; Cahill, P. A. *Appl. Phys. Lett.* **1993**, *63*, 1552.
(20) Smilowitz, L.; Sariciftci, N. S.; Wu, R.; Gettinger, C.; Heeger, A. J.; Wudl, F. *Phys. Rev. B* **1993**, *47*, 13835.
(21) Yoshino, K.; Yin, X. H.; Morita, S.; Kawai, T.; Zakhidov, A. A. *Solid State Commun*. **1993**, *85*, 85.
(22) Morita, S.; Kiyomatsu, S.; Yin, X. H.; Zakhidov, A. A.; Noguchi, T.; Ohnishi, T.; Yoshino, K. *J. Appl. Phys.* **1993**, *74*, 2860.
(23) Silence, S. M.; Scott, J. C.; Stankus, J. J.; Moerner, W. E.; Moylan, C. R.; Bjorklund, G. C.; Twieg, R. J. *J. Phys. Chem.* **1995**, *99*, 4096.
(24) Zhang, Y.; Cui, Y.; Prasad, P. N. *Phys. Rev. B* **1992**, *46*, 9900.
(25) Arbogast, J. W.; Darmanyan, A. P.; Foote, C. S.; Rubin, Y.; Diederich, F. N.; Alvarez, M. M.; Anz, S. J.; Whetten, R. L. *J. Phys. Chem.* **1991**, *95*, 11.
(26) (a) Tanigaki, K.; Ebbesen, T. W.; Kuroshima, S. *Chem. Phys. Lett.* **1991**, *185*, 189. (b) Terazima, M.; Hirota, N.; Shinohara, H.; Saito, Y. *J. Phys. Chem*. **1991**, *95*, 9080.
(27) Dimitrijevic, N. M.; Kamat, P. V. *J. Phys. Chem*. **1992**, *96*, 4811.
(28) Average donor distance is calculated as $V^{1/3}$ where V is the molar volume. The molar volume for PVK is 161 cm^3/mol, from: Bicerano, J. *Prediction of Polymer Properties*; Marcel Dekker: New York, 1993; p 69.
(29) Onsager, L. *Phys. Rev.* **1938**, *54*, 554.
(30) Melz, P. J. *J. Chem. Phys.* **1972**, *57*, 1694.
(31) Yokoyama, M.; Endo, Y.; Mikawa, H. *Bull. Chem. Soc. Jpn.* **1976**, *49*, 1538.

(32) Yokoyama, M.; Endo, Y.; Matsubara, A.; Mikawa, H. *J. Chem. Phys.* **1981**, *75*, 3006.
(33) Yokoyama, M.; Shimokihara, S.; Matsubara, A.; Mikawa, H. *J. Chem. Phys*. **1982**, *76*, 724.
(34) Wang, Y. *Photoconductive Polymers*. In *Kirk-Othmer Encyclopedia of ChemicalTechnology, Fourth Edition*; Wiley: New York, 1996; p 837.
(35) Braun, C. L. *J. Chem. Phys.* **1984**, *80*, 4157.
(36) Noolandi, J.; Hong, K. M. *J. Chem. Phys.* **1979**, *70*, 3230.
(37) Samoc, M.; Williams, D. F. *J. Chem. Phys*. **1983**, *78*, 1924.
(38) Willig, F. *Chem. Phys. Lett.* **1976**, *40*, 331.
(39) Isoda, K.; Kouchi, N.; Hatano, Y.; Tachiya, M. *J. Chem.Phys.* **1994**, *100*, 5874.
(40) Marcus, R. A.; Siders, P. *J. Phys. Chem*. **1982**, *86*, 622.
(41) Marcus, R. A. *Annu. Rev. Phys. Chem*. **1964**, *15*, 155.
(42) Levich, V. G. *Adv. Electrochem. Eng.* **1966**, *4*, 249.
(43) Hush, N. S. *Trans. Faraday Soc*. **1961**, *57*, 557.
(44) Jortner, J. *J. Chem. Phys.* **1976**, *64*, 4860.
(45) Ulstrup, J.; Jortner, J. *J. Chem. Phys*. **1975**, *63*, 4358.
(46) Turro, N. J. *Proc. Natl. Acad. Sci*. **1983**, *80*, 609.
(47) Kaptein, R. *Adv. Free Radical Chem*. **1975**, *5*, 381.
(48) Reference 48.
(49) Wang, Y.; Herron, N. *Chem. Phys. Lett.* **1992**, *71*, 200.
(50) Connors, K. A. In *Binding Constants. The Measurement of Molecular Complex Stability*; John Wiley & Sons: New York, 1987.
(51) Scher, H.; Lax, M. *Phys. Rev*. **1973**, *B7*, 4491, 4502.
(52) Scher, H.; Montroll, E. W. *Phys. Rev*. **1975**, *B12*, 2455.
(53) Bässler, H. *Philos. Mag. B* **1984**, *50*, 347.
(54) Borsenberger, P. M.; Pautmeier, L.; Bässler, H. *J. Chem. Phys.* **1991**, *94*, 5447.
(55) Kepler, R. G.; Zeigler, J. M.; Harrah, L. A.; Kurtz, S. R. *Phys. Rev. B* **1987**, *35*, 2818.
(56) Abkowitz, M.; Knier, F. E.; Yuh, H.-J.; Weagley, R. J.; Stolka, M. *Solid State Commun*. **1987**, *62*, 547.
(57) Stolka, M.; Yuh, H.-J.; McGrane, K.; Pai, D. M. *J. Polym. Sci.: Part A: Polym. Chem*. **1987**, *25*, 823.
(58) Fujino, M. *Chem. Phys. Lett.* **1987**, *136*, 451.
(59) Gill, W. D. *J. Appl. Phys.* **1972**, *43*, 5033.
(60) Pfister, G.; Williams, D. J. *J. Chem. Phys.* **1974**, *61*, 2416.
(61) Melz, P. J. *J. Chem. Phys.* **1972**, *57*, 1694.
(62) Mozumder, A. *J. Chem. Phys.* **1974**, *60*, 4300.
(63) Reimer, B.; Bassler, H. *Phys. Status Solidi A* **1979**, *51*, 445.